Integration of Planar Antennas Considering Electromagnetic Interactions at Board Level

Florian Ohnimus, Gerhard Fotheringham, Ivan Ndip, *Member, IEEE*, A. Ege Engin, *Member, IEEE*, Stephan Guttowski, Herbert Reichl, *Fellow, IEEE*, and Klaus-Dieter Lang, *Member, IEEE*

***Abstract*—In compact wireless modules, electromagnetic (EM) interactions occurring between planar antennas and transmission lines (TML) sharing the same substrate may cause a high amount of undesired coupling and may also detune the antenna characteristics. In this paper, an approach for defining a block-out region around the planar antenna, where no components should be placed is developed, thereby ensuring that the antenna characteristics remain within tolerable limits when the antenna is integrated at board level. This region is comparable to the reactive near-field, but is determined by evaluating the reactive EM power density excited on the ground plane and deducing a threshold value. Its boundary will be termed the EM antenna boundary. Furthermore, a method for efficient estimation of EM coupling from the antenna to terminated TMLs routed outside the EM antenna boundary is developed. This method is based entirely on a postprocessing step to field simulations, i.e., the coupling is calculated based on the previously computed magnetic field distribution excited by the antenna on the ground plane. The coupling model uses the theory of field excited TMLs together with the Baum–Liu–Tesche integral equations for obtaining the terminal voltages of the TML and, hence, the coupling terms.**

***Index Terms*—Electromagnetic (EM) coupling, EM antenna boundary, near-field, planar antennas, planar transmission lines (TMLs), reactive power.**

I. Introduction

THE (quasi) millimeter-wave range provides large spectral bandwidths for wireless short-range microelectronic communication systems. Efficient planar antennas, with dimensions at the order of millimeters, are integrated at board level using printed circuit board (PCB) technologies; thus, facilitating the realization of compact and low-cost wireless modules. Furthermore, the required antenna size for efficient operation scales proportionally with the operating wavelength, potentially allowing a high degree of system miniaturization.

Manuscript received August 24, 2010; revised January 14, 2011 and March 9, 2011; accepted March 12, 2011.

F. Ohnimus, G. Fotheringham, I. Ndip, S. Guttowski, H. Reichl, and K.-D. Lang are with the Fraunhofer Institute for Reliability and Microintegration, 13355 Berlin, Germany, and also with the School of Electrical Engineering and Computer Sciences, Technical University Berlin, 10623 Berlin, Germany (e-mail: florian.ohnimus@izm.fraunhofer.de; gerhard.fotheringham@izm.fraunhofer.de; ivan.ndip@izm.fraunhofer.de; stephan.Guttowski@izm.fraunhofer.de; reichl@izm.fhg.de; lang@izm.fhg.de).

A. E. Engin is with the Department of Electrical and Computer Engineering, San Diego State University, San Diego, CA 92182 USA. (e-mail: aengin@mail.sdsu.edu).

Color versions of one or more of the figures in this paper are available online at http://ieeexplore.ieee.org.

Digital Object Identifier 10.1109/TEMC.2011.2131656

Planar antennas such as patch, slot, and dipole configurations have been predominantly designed and tailored with regard to high gain and high efficiency/bandwidth operation and are manufacturable in low-cost PCB technologies [1]–[4].

Planar transmission lines (TMLs) (e.g., microstrip and coplanar) are typical components required for signal distribution on PCBs. However, their open field nature makes them vulnerable toward undesired electromagnetic (EM) coupling either through neighboring board components, especially antennas, or external fields. To date, single and coupled TMLs have been thoroughly modeled and analyzed [5]–[8]. Based on the telegrapher's equations, analytical approaches as well as simulation techniques have been employed to extract the propagation constant γ and characteristic impedance Z_0 as well as the per-unit-length parameters. Coupling of external fields to TMLs has also been extensively analyzed. Formulations for the equivalent sources of the inhomogeneous telegrapher's equations of TMLs when illuminated by an external EM field have been developed [9]–[11]. Together with the Baum–Liu–Tesche (BLT) integral equations, coupling to the TMLs has been calculated [12] in the case of plane wave illumination. Leone [13], [14] applied the BLT equations to study the impact of externally illuminated fields on the terminal response of microstrip lines as well as the EM radiation from PCB traces.

Integrated antennas have been modeled considering both coupling between antenna elements for array applications [15]–[18] as well as between antennas and board components. For example, in [19], the EM interactions between microstrip lines integrated in close proximity to patch antennas for 2.4-GHz applications were studied and design guidelines to minimize EM interactions were derived. In [20], an approach for assessing coupling between integrated mobile phone antennas and PCB TMLs together with a fitting algorithm is proposed. Techniques for reducing mutual coupling [21], [22] between antennas have also been proposed and studied.

Despite these contributions made so far, the EM interactions of excited antenna fields with neighboring TMLs, which may potentially also result in degradation of the antenna characteristics if the TML is routed too close to the antenna, have not been analyzed in the (quasi) millimeter-wave range. Furthermore, although methods for calculating coupling between TMLs (crosstalk) and from external fields to TMLs have been presented, methods for efficiently estimating the coupling between planar antennas and TMLs sharing the same substrate, as an alternative to time-consuming complete full-wave EM field simulations, have not been investigated. Therefore, this

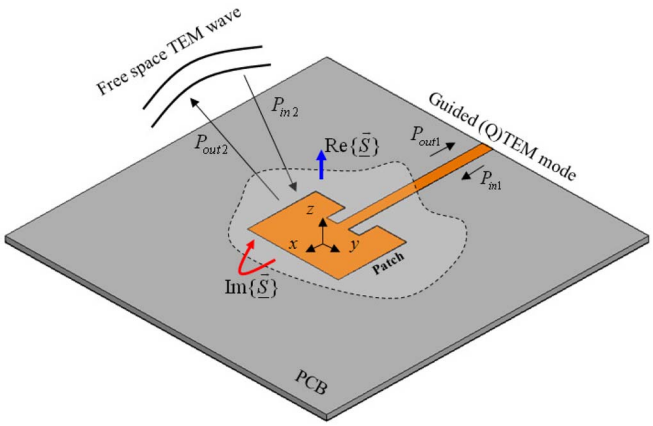

Fig. 1. Illustration of the complex power density transfer to and from a planar antenna configuration integrated on a PCB.

contribution addresses the following aspects concerning planar antenna integration at board level:

1) Development of an approach for defining the block-out region around the antenna, bounded by the EM antenna boundary, where no components should be placed, thereby ensuring that the antenna characteristics remain within tolerable limits (see Section II).
2) Development of a method for efficient calculation of coupling from the antenna fields to TMLs routed on the same substrate outside the EM antenna boundary (see Section III).

Based on the proposed approach and method, numerical full-wave simulation efforts are reduced during the integration of planar antennas. To illustrate this, the proposed approach and method are quantified by considering a patch antenna on a grounded substrate and microstrip TMLs routed in close proximity as an example.

II. Approach to Define EM Antenna Boundary

Defining the electrical boundaries of board components enables them to be analyzed independently without considering the impact of other components in the immediate vicinity. This leads to a better understanding of their electrical behavior and also facilitates the development of design rules for integration. The concept of defining the electrical boundaries of packaging structures was first introduced in [23] and [24]. The main idea is that the electrical length of a component extends until the reactive power excited by the component (through higher order modes) "diminishes." In these works, a methodology was developed and illustrated for defining the boundaries of geometrical discontinuities, such as TML bends, vias, bumps, etc. However, integrated planar antennas have not been considered so far.

Consider an excited patch antenna on a grounded dielectric substrate for low-cost PCB applications, as shown in Fig. 1.

The power density $\underline{\vec{S}}$ (Poynting vector) exits or enters the volume around the antenna. P_{in1} and P_{out1} are the input and output powers of the quasi-TEM (QTEM) mode on the TML, and P_{in2} and P_{out2} are the input and output powers of the TEM space wave mode in the far-field of the antenna, respectively. The mode conversion occurs in the antenna structure, where a resonance mode is excited.

The antenna radiates a portion of the power (indicated by $\mathrm{Re}\{\underline{\vec{S}}\}$) in the lateral plane on the substrate, where other board components could be placed. Furthermore, as a result of an enforced resonance condition on the planar antenna (resonator), the stored energy in the near-field region is high. This is indicated by the reactive power density $\mathrm{Im}\{\underline{\vec{S}}\}$. The antenna parameters depend primarily on the near-field distribution. Intuitively, the near-field region is larger than the geometrical dimensions of the antenna, loosely indicated by the dashed bounded region around the antenna structure. The EM fields excited on components placed on the substrate close to the antenna interact with the near-field distribution potentially also altering the antenna parameters, as has been shown in [19]. Therefore, it is desirable to determine a block-out region around the antenna within which no other board components should be placed. In Section II-A, an approach for this purpose is developed.

A. Basic Idea and Overview of Approach

The reactive near-field region is defined as the portion of the near-field immediately surrounding the antenna, wherein the reactive field is dominant [25]. Since the reactive field decays much more rapidly than the radiation field, the boundary of the reactive near-field should provide a plausible definition for the antenna's EM boundary. Unfortunately, the ideal infinitesimal dipole is practically the only antenna type, where this region can be given precisely. The conventional reactive near-field boundary is given as the radian sphere with radius equal to the radian distance $r = \lambda/2\pi$. For electrically large antennas, the boundary of the reactive near-field is commonly taken to exist at a distance $r = 0.62(d^3/\lambda)^{1/2}$ from the antenna surface, where d is the largest dimension of the antenna, provided that d is large compared to the wavelength [25]. But this need not be the case for planar antennas. Furthermore, in a practical application, this critical near-field region defined as such may be larger than required, hence, unnecessarily wasting available board space. Besides, defining a "radius" does not seem to be appropriate for planar antennas. Therefore, a novel approach for determining the boundary of the reactive near-field and, thus, defining the EM antenna boundary is proposed. The basic idea is not to specify a distance directly, but to determine a threshold value of the reactive power density by directly evaluating $\mathrm{Im}\{\underline{\vec{S}}\}$. A 2-D block-out region in the lateral plane is desired in the context of planar antennas. Therefore, the considerations will be restricted to the substrate of the antenna. Since the substrate is generally electrically thin, the values of the fields do not change in the direction of the z-axis within the substrate, i.e., they are assumed approximately the same on the top and bottom planes.

The determination of the EM antenna boundary is based on the known complex EM field distribution, specifically in the near-field of the antenna. Since full-wave EM solvers are mostly used in practice during the design of antennas, the complex field distribution is available once the antenna has been simulated. An overview of the proposed approach is illustrated in Fig. 2.

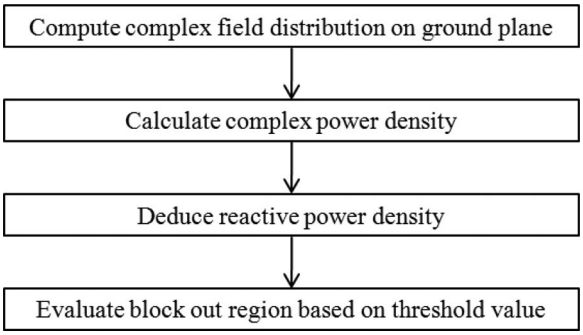

Fig. 2. Overview of approach to determine the EM antenna boundary.

In the first step, the excited fields of the planar antenna are computed on the ground plane using full-wave field simulations. These comprise the tangential magnetic field components $\underline{H}_x$ and $\underline{H}_y$, and the normal electric field component $\underline{E}_z$. In this case, the complex power density $\underline{\vec{S}}$ can be written as follows:

$$\underline{\vec{S}} = \frac{1}{2}(\underline{\vec{E}} \times \underline{\vec{H}}^*) = -\frac{1}{2}\left(\underline{E}_z \underline{H}_y^* \vec{e}_x - \underline{E}_z \underline{H}_x^* \vec{e}_y\right). \quad (1)$$

From (1), the reactive power density $|\mathrm{Im}\{\underline{\vec{S}}\}|$ is evaluated and a threshold value $|\mathrm{Im}\{\underline{\vec{S}}\}|_{\max}$ is deduced. The block-out region is then defined as the set of all points in the plane for which $|\mathrm{Im}\{\underline{\vec{S}}\}| > |\mathrm{Im}\{\underline{\vec{S}}\}|_{\max}$. Accordingly, the EM antenna boundary is defined as follows:

$$|\mathrm{Im}\{\underline{\vec{S}}\}| \quad \left\{ \begin{array}{l} > |\mathrm{Im}\{\underline{\vec{S}}\}|_{\max}, \text{ inside EM antenna boundary} \\ < |\mathrm{Im}\{\underline{\vec{S}}\}|_{\max}, \text{ outside EM antenna boundary} \end{array} \right\}. \quad (2)$$

We considered different approaches for defining the threshold value. Since the reactive power density has a faster spatial decay rate in comparison to the propagating power density, a maximum ratio could be defined as $|\mathrm{Im}\{\underline{\vec{S}}\}|/|\mathrm{Re}\{\underline{\vec{S}}\}|$, or a maximum tolerable limit of $|\mathrm{Im}\{\underline{\vec{S}}\}|$ could be given directly. However, these limits do not consider the antenna parameters including the resonance frequency, antenna efficiency, and input reflection coefficient, as well as the input power, which all take direct influence on the reactive near-field distribution and, hence, the reactive power density.

Therefore, the approach we pursue in the following is to seek the analogy to the ideal infinitesimal dipole and also to include the antenna parameters and input power in order to set up a generalized expression for the threshold value. In the case of the ideal infinitesimal dipole, the averaged radial components of the reactive and propagating power densities at the radian distance $r = \lambda/2\pi$ are equal and assume the following value:

$$|\mathrm{Im}\{\underline{\vec{S}}\}|_{\max} = \frac{\pi P_{\mathrm{out2}}}{\lambda^2}. \quad (3)$$

The threshold value (3) defined as such is related to the power exiting the antenna structure P_{out2} and the wavelength λ. If (3) is expressed in terms of the input power of the antenna P_{in1}, the antenna efficiency η and the input reflection coefficient S_{11} of the antenna are considered

$$|\mathrm{Im}\{\underline{\vec{S}}(P_{\mathrm{in1}}, \eta, S_{11})\}|_{\max} = \frac{\pi P_{\mathrm{in1}}}{\lambda^2}(1 - |S_{11}|^2)\eta. \quad (4)$$

The actual power delivered to the antenna is contained in the term $1 - |S_{11}|^2$ considering impedance mismatch with the feeding line. The power contained in the near-fields including the power loss (conductor and dielectric losses) is given by η. The threshold value (4) can be considered a more natural definition, since it is based on the analogy to the reactive near-field boundary of the ideal infinitesimal dipole and also includes input power and the antenna specific parameters. Fig. 3 shows a graphical illustration of the computed reactive power density of the patch antenna with its fast spatial decay rate as well the threshold value defined in the 2-D plane of the substrate.

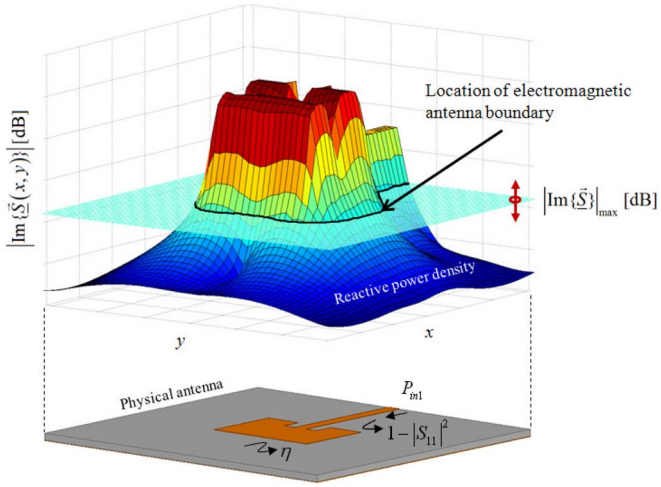

Fig. 3. Graphical illustration of the reactive power density, the threshold value for determining the electromagnetic antenna boundary, as well as the required antenna parameters.

Regions around the excited antenna with higher reactive power density than given in (4) are, hence, inside the antenna boundary and should be considered as part of the antenna structure. Components placed inside the antenna boundary have influence on the antenna near-field distribution and may change the antenna characteristics.

B. Illustration of Approach

The approach for defining the EM antenna boundary is shown and compared to the conventional definition of the antenna near-field region by considering a patch antenna and microstrip TML sharing the same substrate.

The components are designed for 24 GHz operation on a typical high-frequency PCB with $\varepsilon_r = 3.75$, $\tan(\delta) = 0.006$, a substrate height of $h = 250$ μm, and a metallization thickness of $t = 17.5$ μm. The copper metallization has a conductivity of 58 MS/m. The parameters of the designed microstrip TML and patch antenna are presented in Section II-B1 and 2. The antenna boundary is deduced in Section II-B3 and studies of the TML spacing are conducted.

1) Microstrip-Line Parameters: Fig. 4 shows the cross section of a microstrip TML routed on the grounded substrate. It

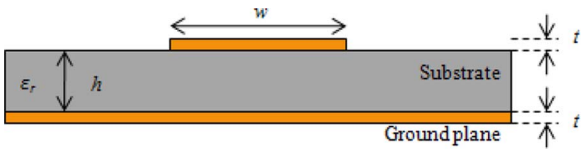

Fig. 4. Cross section of a microstrip line on a grounded substrate with dimensions.

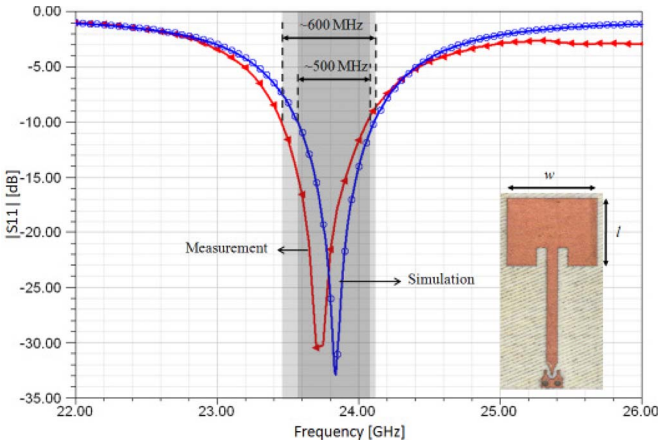

Fig. 5. Simulation and measurement results of the 24-GHz patch antenna.

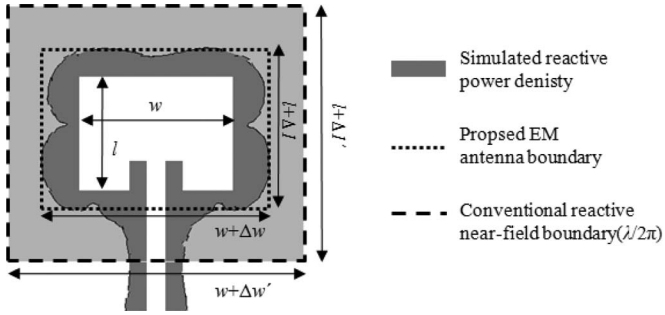

Fig. 6. Simulated reactive power density on the ground plane of the patch antenna.

TABLE I
COMPARISON OF ELECTRICAL ANTENNA SIZES AS DEFINED BY CONVENTIONAL REACTIVE NEAR-FIELD BOUNDARY AND THE PROPOSED EM ANTENNA BOUNDARY

Boundary type	Distance from antenna	
	Δl [mm]	Δw [mm]
Conventional "textbook" reactive near-field boundary	4	4
Proposed EM antenna boundary	1.4	2.2

will be used in this example. The height h and parameters of the substrate are identical to those of the patch antenna.

The TML parameters were computed using a 2-D quasi-static solver. For the target characteristic impedance of 50 Ω, a width $w = 500$ μm was determined. The computed per-unit-length inductance L' and per-unit-length capacitance C' are 295 nH/m and 110 pF/m, respectively.

2) Patch Antenna Parameters: The patch antenna depicted in Fig. 5 comprises a metallic patch above a ground plane excited with its fundamental λ/2 resonance mode (lowest order TM mode). The patch length l and width w are tuned for operation at 24 GHz. The dimensions $l = 3.175$ mm and $w = 4.25$ mm were determined after optimization.

For the EM field simulations, Ansys HFSS v12, a 3-D full-wave solver based on the finite-element method (FEM), was used. An inset feed is used so that the microstrip line can be placed on the same layer as the patch. The length of the inset and the width of the gaps are optimized to ensure impedance matching to the 50-Ω microstrip line at 24 GHz. This antenna as well as its excited field distribution has been analyzed in [1].

In order to experimentally characterize the input reflection coefficient and impedance bandwidth of the antenna, a test structure was manufactured and measured. The measurement results are compared to simulations. Fig. 5 shows the measured reflection coefficient S_{11} and a comparison with full-wave simulation as well as a photo of the manufactured antenna. The GSG (ground, signal, and ground) probe adapter at the end of the feeding line is not deembedded from the measurements. The vector network analyzer is, however, calibrated to the tips of the GSG probes. A slight discrepancy in resonance frequency is observed. The higher measured bandwidth of 600 MHz compared to 500 MHz is primarily caused by additional losses, such as the surface roughness of the copper. Nevertheless, it is observed that the antenna operates at 24 GHz.

3) Deduction of EM Antenna Boundary: The antenna boundary is deduced for the patch antenna configuration. For this purpose, the Poynting vector (1) and the reactive power density threshold (4) are evaluated based on the simulated field distribution. The antenna is fed with $P_{\mathrm{in}1} = 1$ mW input power. The antenna efficiency $\eta = 82\%$ was also determined by full-wave simulation. Since the antenna exhibits a small reflection coefficients < -10 dB at 24 GHz, S_{11} can be neglected.

The resulting reactive power density threshold value from (4) is 16 μW/mm^2. In Fig. 6, the simulated reactive power density with the threshold value in the 2-D plane is shown.

The EM antenna boundary is located on the isoline of the reactive power density threshold according to (3). Please note that the block-out area so defined is not rectangular. For practical design guidelines, it is advantageous to work with the circumscribed rectangle. The geometrical parameters Δl, $\Delta l'$ and Δw, $\Delta w'$ are introduced to describe the electrical size increase compared to the physical antenna length l and antenna width w, respectively. The inner rectangle defines the proposed EM antenna boundary. The outer rectangle defines the conventional textbook reactive near-field boundary located at $r = \lambda/2\pi$ from the antenna surface/edge [25]. Table I shows the comparison between the conventional reactive near-field boundary and the EM antenna boundary proposed in this paper.

In order to show the feasibility of using the antenna boundary for the integration of planar antennas, it is necessary to study the effects of nonresonant TMLs placed inside this boundary on the antenna parameters.

Fig. 7 shows an illustration of the patch antenna with additional microstrip TMLs routed within the antenna boundary. At the ends, the TMLs are matched terminated such that only

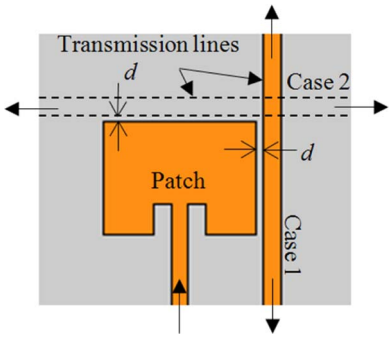

Fig. 7. Illustration of the patch antenna with microstrip TMLs routed inside the antenna boundary.

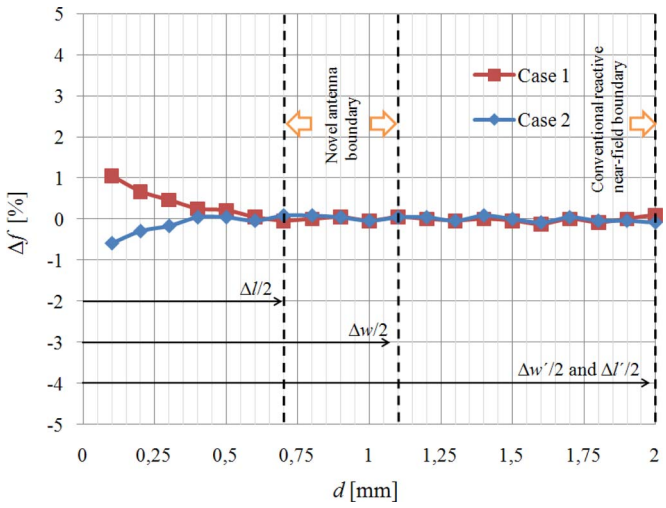

Fig. 8. Effects of the microstrip TML routed inside the antenna boundary on the resonance frequency of the patch antenna.

minimal reflections occur. Standing waves on the TML are, thus, small.

Fig. 8 shows the simulated change in resonance frequency Δf of the patch antenna for different TML edge-to-edge separation distances d.

It is observed that the resonance frequency of the patch antenna changes for small values of d when the TML is brought closer by 1% and -0.6% for cases 1 and 2, respectively. This attributes to parallel inductive loading (case 1) and shunt capacitive loading (case 2) of the TML in the antenna near-field. With increasing values of d, Δf eventually settles to a constant value, and the secondary fields excited on the TML by the antenna can be assumed to have negligible effect on the primary antenna fields. It is also observed that the antenna boundary indicated in Fig. 8 can be used to determine a critical region (or blockout area) around the physical antenna structure, where the TML should not be routed. Therefore,

1) TMLs can be safely integrated when routed outside the EM antenna boundary, i.e., the effects of the TML on the antenna performance can be neglected in this case;
2) if, however, TMLs are to be routed inside the EM antenna boundary, the fields need to be recomputed, since the TML, in this case, needs to be considered as being "part" of the antenna.

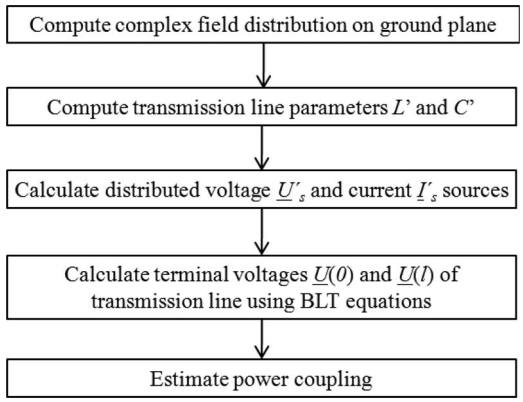

Fig. 9. Overview of method to calculate coupling from the antenna to TMLs.

It is also observed that the antenna boundary defines a region around the antenna, which is significantly smaller than the conventional reactive near-field boundary defined in literature. This is important for applications with high integration densities.

Although TMLs can be integrated outside the EM antenna boundary without significantly affecting the antenna performance, antenna field coupling to TMLs routed on the same substrate still occurs. Therefore, in Section III, a method to efficiently calculate this coupling is proposed.

III. Method to Calculate Coupling to TMLs

In this section, an overview of the proposed method to quantify coupling is given. With this method, coupling to TMLs routed outside the EM antenna boundary can be calculated. Similarly to the work in [20], the basic idea is to compute the antenna fields first with no TMLs in the vicinity of the antenna. This is practical, since the antenna is typically designed on the substrate configuration prior to component placement and TML routing. If the TML is routed outside the antenna boundary, the weak coupling assumption can be made, i.e., the secondary fields excited on the TMLs by the primary antenna fields have negligible influence on the antenna parameters. It should also be noted that the coupling is nevertheless reciprocal assuming that all materials are linear and isotropic.

A. Derivation of Coupling Model

Fig. 9 shows an overview of the proposed method for calculating coupling between planar antennas and TMLs. Assuming a good ground plane conductor, the magnetic field components tangential to and on the ground plane $\underline{H}_x$ and $\underline{H}_y$ are computed first for the designed antenna configuration using a full-wave EM field solver. These are the source fields for determining the coupling to the TML. Note that the source fields are determined with no TMLs present on the substrate. Although either the electric or magnetic field can be used, which are directly related through Maxwell's equations, the tangential magnetic field components are chosen because they are well defined tangential to the ground plane through the surface currents excited by the

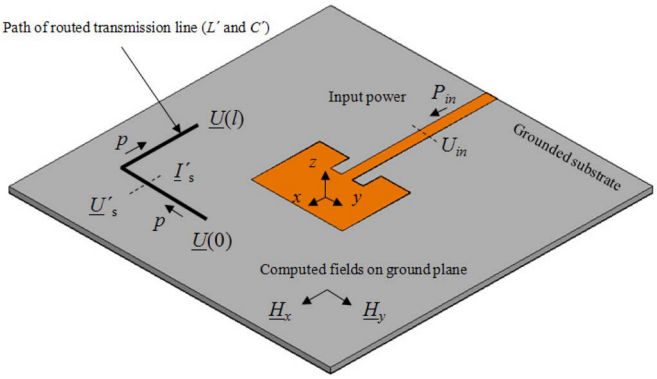

Fig. 10. Illustration of method to calculate coupling from antenna fields to TMLs.

antenna. In practical PCB applications, nonpermeable dielectric materials are used with $\mu_r = 1$.

Next, the TML parameters L' and C' of the TML that is to be routed on the substrate next to the antenna are computed using a 2-D quasi-static or full-wave solver. Typical microstrip TMLs routed on low-loss substrates have a small attenuation constant α, i.e., the per-unit-length series resistance and the per-unit-length shunt conductance are small.

Fig. 10 shows an illustration of a possible TML routing path on the substrate near the planar antenna and the described parameters.

Based on the desired routing path of the TML, the distributed voltage $\underline{U}'_s$ and current $\underline{I}'_s$ sources along the TML are determined. These sources are determined in terms of

1) the magnetic field components $\underline{H}_x$ and $\underline{H}_y$;
2) the curl $\vec{\nabla} \times (\underline{H}_x \vec{e}_x + \underline{H}_y \vec{e}_y)$ on the ground plane.

Since the distributed sources also satisfy the inhomogeneous Telegrapher's equations of the TML, the BLT equations [12] are used to calculate the terminal voltages $\underline{U}(0)$ and $\underline{U}(l)$ by line integration of the distributed sources along the path p of the TML. The letter p will be used as the natural parameterization $(0 \leq p \leq l)$ for the TML routing path. Finally, together with the antenna input voltage U_{in} on the feeding line, the coupling terms between the antenna port and TML ports are calculated.

In the following, equations for linking the computed field distribution of the antenna to the equivalent sources on the TML are derived. The inhomogeneous Telegrapher's equations are written with distributed voltage and current source terms $\underline{U}'_s(p)$ and $\underline{I}'_s(p)$ in dependency of the angular frequency ω and per-unit-length TML parameters L' and C' [12]

$$\frac{d\underline{U}(p)}{dp} + j\omega L' \underline{I}(p) = \underline{U}'_s(p) \tag{5}$$

$$\frac{d\underline{I}(p)}{dp} + j\omega C' \underline{U}(p) = \underline{I}'_s(p). \tag{6}$$

Here, $\underline{U}'_s(p)$ and $\underline{I}'_s(p)$ represent the distributed sources due to the exciting antenna fields on the ground plane. Again, note that the fields of these sources are generated in the absence of the TML.

Next, it is assumed that the TML, which is to be routed on the substrate, has low loss so that the per-unit-length resistance R' and the per-unit-length conductance G' are negligible. The impedance of the TML is then real and given by the high-frequency limit

$$Z_0 = \sqrt{\frac{L'}{C'}}. \tag{7}$$

The distributed sources along the TML routing path p are approximated in dependency of the antenna fields. Applying Maxwell's first two equations (Ampere's and Faraday's laws), the distributed sources can be expressed in terms of the external incident fields [12]. The substrate parameters are specified with the permeability μ_0 and permittivity $\varepsilon = \varepsilon_0 \varepsilon_r$

$$\underline{U}'_s(p) = -j\omega\mu_0 h \underline{H}_\perp(p) \tag{8}$$

$$\begin{aligned} \underline{I}'_s(p) &= -j\omega C' h \underline{E}_z(p) \\ &= -\frac{C'h}{\varepsilon}\left(\frac{\partial}{\partial x}\underline{H}_y(p) - \frac{\partial}{\partial y}\underline{H}_x(p)\right). \end{aligned} \tag{9}$$

Note that $\underline{H}_\perp(p)$ is introduced describing the magnetic field component orthogonal to the TML path p. Furthermore, the current source (9) is expressed in terms of the exciting magnetic field. Note that these distributed sources are functions of the position of the TML. The spatial dependency of the magnetic field in the substrate may be assumed constant for $0 < z < h$. This is only valid for electrically "short" substrate heights $\lambda \gg h$. Furthermore, it is assumed that the tangential electric and normal magnetic field components are zero on the ground plane, which is valid for high ground plane conductivities.

The distributed sources now need to be integrated along the TML routing path p considering the phase constant and impedance of the TML. For this purpose, the BLT equations are used [12] yielding the source terms $\underline{S}_1$ and $\underline{S}_2$

$$\underline{S}_1 = \frac{1}{2}\int_0^l \left(\underline{U}'_s(p) + Z_0 \underline{I}'_s(p)\right) \exp(j\beta p) dp \tag{10}$$

$$\underline{S}_2 = -\frac{1}{2}\int_0^l \left(\underline{U}'_s(p) - Z_0 \underline{I}'_s(p)\right) \exp(j\beta l - j\beta p) dp. \tag{11}$$

L', C', and the phase constant $\beta = 2\pi f\ (L'C')^{0.5}$ of the TML must be known. The BLT equations can be interpreted as a summation of the exciting antenna fields, i.e., the distributed voltage and current sources along the TML. For further simplicity, it is assumed that the TML is matched at both ends such that only minor reflections are encountered and, hence, the standing wave ratio on the TML is small. This assumption is valid in practical applications with impedance-controlled design. Expanding (10) and (11), and relating them to the terminal voltages $\underline{U}(p = 0)$ and $\underline{U}(p = l)$ results in the following:

$$\begin{aligned} \underline{U}(p=0) = {} & \frac{j\omega\mu_0 h}{2}\exp(j\beta l)\int_0^l \underline{H}_\perp(p)\exp(-j\beta p)dp \\ & - \frac{C'h}{2\varepsilon} Z_0 \exp(j\beta l)\int_0^l \left(\frac{\partial}{\partial x}\underline{H}_y(p) - \frac{\partial}{\partial y}\underline{H}_x(p)\right) \\ & \times \exp(-j\beta p)dp \end{aligned} \tag{12}$$

$$\underline{U}(p=l) = -\frac{j\omega\mu_0 h}{2}\int_0^l \underline{H}_\perp(p)\exp(j\beta p)dp - \frac{C'h}{2\varepsilon}Z_0\int_0^l\left(\frac{\partial}{\partial x}\underline{H}_y(p) - \frac{\partial}{\partial y}\underline{H}_x(p)\right) \times \exp(j\beta p)dp. \quad (13)$$

These equations can be evaluated entirely in a postprocessing step to full-wave simulations of the antenna fields. By relating the terminal voltages at the TML start and end points, $\underline{U}(p=0)$ and $\underline{U}(p=l)$, respectively, to the antenna feeding line voltage U_{in} the coupling terms $|S_{12}|$ and $|S_{13}|$ between the antenna and TML are obtained

$$|S_{12}|[\text{dB}] = 20\log\left(\frac{|\underline{U}(p=0)|}{U_{\text{in}}}\right) \quad (14)$$

$$|S_{13}|[\text{dB}] = 20\log\left(\frac{|\underline{U}(p=l)|}{U_{\text{in}}}\right). \quad (15)$$

Only the magnitude of the coupling is of interest. Therefore, the phase is suppressed at this stage. Furthermore, U_{in} can be expressed in terms of the input power P_{in} and the feeding line impedance Z_0

$$U_{\text{in}} = \sqrt{2P_{\text{in}}Z_0}. \quad (16)$$

The formulations and simplifications presented in this section allow the calculation of coupling from the antenna fields to TMLs without performing additional full-wave simulations for each TML routing path. Since the coupling is reciprocal, it is valid for both directions, i.e., from the antenna port to the TML ports and from the TML ports to the antenna port. Therefore, it is sufficient to compute the tangential magnetic fields excited by the antenna on the ground plane once, and then, perform a postfield integration. In the following, a summary of the simplifications and assumptions is given.

1) Weak coupling is assumed, i.e., the secondary fields excited on the TMLs have no influence on the primary antenna fields. In other words, the TML must be routed outside the EM antenna boundary.
2) QTEM wave propagation is assumed on the TML, so that it can be modeled with the per-unit-length parameters.
3) The effects of TML discontinuities are assumed to have negligible influence of the propagation of the QTEM mode in comparison to a straight TML.
4) Only the tangential magnetic field components on the ground plane are evaluated to determine the coupling. The normal magnetic field component is assumed zero. This is only valid for high ground plane conductivity values.
5) The spatial dependency of the magnetic field in the substrate is assumed negligible for $0 < z < h$. This is only valid for electrically "short" substrate heights $\lambda \gg h$.
6) The TML is assumed matched at both terminals. Therefore, standing waves and resulting TML resonances are assumed negligible.
7) TML losses are assumed to be small, i.e., $\omega L' \gg R'$ and $\omega C' \gg G'$.

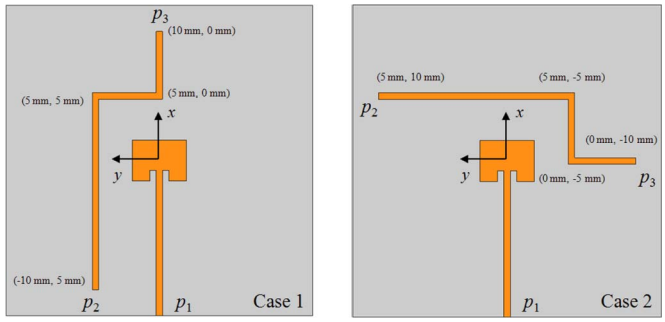

Fig. 11. Illustration of the TML routing path for cases 1 and 2 with the x–y coordinates of the TML specified at the corner and end points.

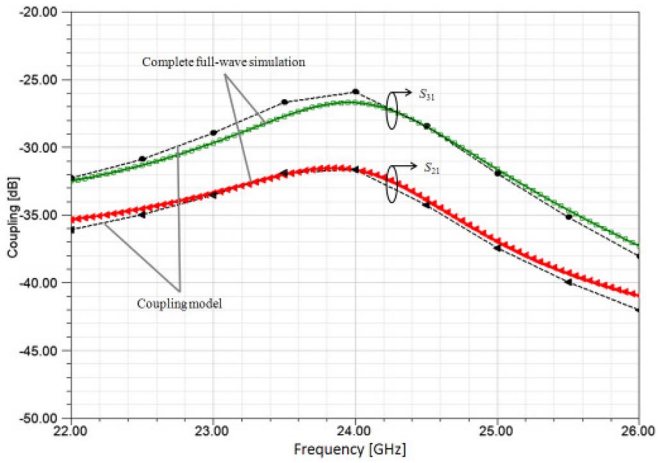

Fig. 12. Comparison of coupling to the TML using the coupling model and complete full-wave simulation for case 1.

Consequently, the accuracy of the coupling model needs to be quantified and compared to complete full-wave simulation and measurement results. This is done in Section III-B.

B. Evaluation of Coupling to TMLs

The coupling method is quantified by considering a microstrip TML routed outside the antenna boundary of the patch antenna. Fig. 11 shows two possible TML routing paths in the vicinity of the patch antenna (cases 1 and 2).

The antenna is driven through a microstrip line at port 1 (p_1) with an input power of 0 dBm from a 50 Ω source. This corresponds to $P_{\text{in}} = 1$ mW. The TML terminals are located at port 2 (p_2) and port 3 (p_3). The total length of the TML is 25 mm. This corresponds to $2\lambda_0$, i.e., an electrically long TML is used in the examples. The terminating loads of the TMLs are set to 50 Ω.

The coupling between the antenna and TML is fully described by the S-parameters S_{21} and S_{31} assuming that all materials are isotropic and linear. Figs. 12 and 13 show the results as predicted by the coupling model compared to the results of the complete full-wave simulation. The frequency response was obtained with the fast sweep implemented in High Frequency Structure Simulator (HFSS), which extrapolates the solution over the desired bandwidth.

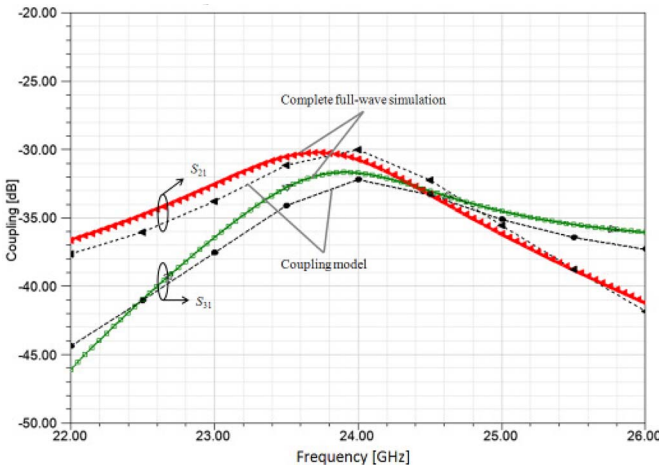

Fig. 13. Comparison of coupling to the TML using the coupling model and complete full-wave simulation for case 2.

Consider the results for case 1. The coupling is largest at the resonance frequency of the antenna, where the excited fields have maximum magnitude. It is observed that the coupling to p_3 is larger than the coupling to p_2. The predicted coupling values by field integration are accurate within 1 dB compared to the complete full-wave simulation across the entire spectrum of interest.

Next, consider the results for case 2. Again, a satisfactory correlation between the field integration and full-wave simulation results is obtained across the entire frequency span. A maximum deviation of 2 dB is observed. The coupling to p_2 is slightly higher than to p_3.

The predicted values of the coupling model match well with the simulations. The coupling is maximal at the resonance frequency of the patch antenna. At this frequency, the magnitude of the magnetic field excited by the patch antenna on the ground plane is particularly high. A typical example of the minimum isolation for the integrated antenna is given in [26]. Here, a maximum tolerable coupling value of -30 dB is required to obtain the desired bit error rate (BER) of 10^{-6} at the receiver.

C. Measurement Results

A comparison between the results of the coupling model, the results of a complete full-wave simulation and measurement results is conducted in this section. Fig. 14 shows photos of two test structures (a) and (b) that were designed and manufactured on the same substrate configuration as the antenna and TML in the previous section.

The antenna and TMLs were contacted with GSG probes. At the ports p_1, p_2, and p_3, probe adapters were designed. These comprise three pads, two of which are shorted to the ground plane with vias. Since the TMLs are placed close to the antenna, it is necessary to ensure that the probe adapters are not too close to the patch antenna so that stray antenna fields do not couple strongly to the GSG probes and, hence, falsify the measurement results. Furthermore, the probe positioners of the network analyzer are orientated orthogonally to one another. Therefore, the probe adapters also need to be orientated orthogonally to one another. For these two reasons, the bends were introduced at the ends of the microstrip lines to facilitate the contacting with the GSG probes.

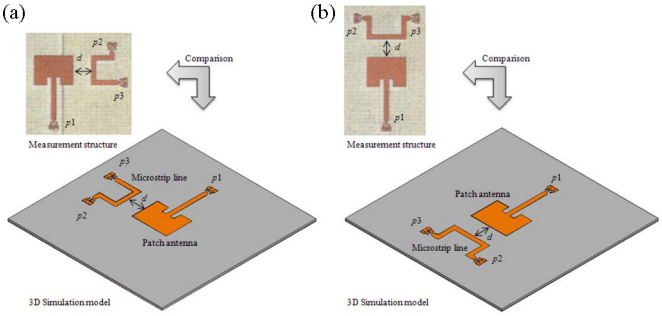

Fig. 14. Photos and simulation models of the test structures used for the S-parameter measurements ($d = 2$ mm).

TABLE II
COMPARISON OF THE CALCULATED, SIMULATED, AND MEASURED COUPLING VALUES BETWEEN THE PATCH ANTENNA AND MICROSTRIP LINE AT 24 GHZ

	Test structure (a)		**Test structure (b)**	
	$\lvert S_{12}\rvert$ [dB]	$\lvert S_{13}\rvert$ [dB]	$\lvert S_{12}\rvert$ [dB]	$\lvert S_{13}\rvert$ [dB]
Model	-28	-29	-32	-32
Simulation	-31	-29	-30	-30
Measurement	-31	-28	-29	-29

Table II shows a summary of the measured coupling values of the test structures and a comparison to the results of the coupling model and complete full-wave simulations. Note that the effects of the GSG probe adapters are not included in the coupling model, in which an ideal termination is assumed.

A discrepancy of up to 3 dB is observed between the calculated values based on the coupling model, and the simulation and measurement results. This is traced back to the parasitics of the GSG probe adapters and GSG probes themselves, which also couple to the fields. However, the measured coupling values match well with the results from the complete full-wave simulations. A discrepancy of 1 dB is observed. The slight differences in measured and simulated data are also due to numerous effects. Influence factors include calibration inaccuracies, influences of the GSG probes, and technological fluctuations. It must be considered that the excited antenna fields do not only couple to the TMLs but also directly to the GSG probes. Nevertheless, the simulation and measurement results match well.

IV. CONCLUSION

This paper focused on two aspects for facilitating efficient planar antenna integration at board level: 1) the EM antenna boundary for planar antennas was determined defining the "block-out" region on the board around the antenna within which no components should be placed in order to ensure that the antenna characteristics remain within tolerable limits; and 2) a method for calculating coupling to TMLs routed outside the antenna boundary was developed allowing efficient evaluation of coupling in the postprocess to 3-D full-wave EM field simulations. Based on the proposed approach and method in this paper, numerical full-wave simulation efforts are reduced during the integration of planar antennas.

REFERENCES

[1] F. Ohnimus, I. Ndip, E. Engin, S. Guttowski, and H. Reichl, "Comparison of electromagnetic field distribution in vicinity of patch and slot antennas," in *Proc. Loughborough Antennas Propag. Conf.*, 2009, pp. 649–652.

[2] F. Ohnimus, A. Podlasly, J. Bauer, A. Ostmann, I. Ndip, S. Guttowski, and H. Reichl, "Electrical design and characterization of elevated antennas at PCB-level," in *Proc. Electron. Compon. Technol. Conf.*, 2009, pp. 1618–1623.

[3] S. Holzwarth and L. Baggen, "Planar antenna design at 60 GHz for high date rate point-to-point connections," in *Proc. Antennas Propag. Soc. Int. Symp.*, 2005, pp. 346–349.

[4] P. R. Grajek, B. Schoenlinner, and G. M. Rebeiz, "A 24-GHz high-gain Yagi-Uda antenna array," *IEEE Trans. Antennas Propag.*, vol. 52, no. 5, pp. 1257–1261, May 2004.

[5] B. C. Wadell, *Transmission Line Design Handbook*. Norwood, MA: Artech House, Inc., 1991.

[6] L. Rubin, "Efficient conformal mapping technique for general transmission line parameter extraction," *IEEE Trans. Magn.*, vol. 29, no. 2, pp. 1380–1384, Mar. 1993.

[7] M. Kang, D. Jang, K. Park, C. Gwon, K. Kim, J. Lim, K. Choi, and D. Ahn, "A new extraction method of characteristic parameters of a coupled transmission line," in *Proc. Electr. Perform. Electron. Packag. Syst.*, Oct. 19–21, 2009, pp. 187–190.

[8] E.-X. Liu, E.-P. Li, and L.-W. Li, "Extraction of circuit parameters for transmission lines by compact 2D FDFD method," in *Proc. Electromagn. Compat.*, Feb. 27, 2006, pp. 188–191.

[9] A. K. Agrawal, H. J. Price, and S. H. Gurbaxani, "Transient response of multiconductor transmission lines excited by a nonuniform electromagnetic field," *IEEE Trans. Electromagn. Compat.*, vol. 22, no. 2, pp. 119–129, May 1980.

[10] C. W. Harrison and C. D. Taylor, "Response of a terminated transmission line excited by a plane wave field for arbitrary angles of incidence," *IEEE Trans. Electromagn. Compat.*, vol. 15, no. 3, pp. 118–120, Aug. 1973.

[11] F. Rachidi, "Formulation of the field-to-transmission line coupling equations in terms of magnetic excitation field," *IEEE Trans. Electromagn. Compat.*, vol. 35, no. 3, pp. 404–407, Aug. 1993.

[12] F. M. Tesche, M. V. Ianoz, and T. Karlsson, *EMC Analysis Methods and Computational Techniques*. Hoboken, NJ: Wiley, 1997.

[13] M. Leone, "Closed-form expressions for the electromagnetic radiation of microstrip signal traces," *IEEE Trans. Electromagn. Compat.*, vol. 49, no. 2, pp. 322–328, May 2007.

[14] M. Leone and H. L. Singer, "On the coupling of an external electromagnetic field to a printed circuit board trace," *IEEE Trans. Electromagn. Compat.*, vol. 41, no. 4, pp. 418–424, Nov. 1999.

[15] D. Pozar, "Considerations for millimeter wave printed antennas," *IEEE Trans. Antennas Propag.*, vol. 31, no. 5, pp. 740–747, Dec. 1983.

[16] H. Wang, D. G. Fang, Y. P. Xi, C. Z. Luan, and B. Wang, "On the mutual coupling of the finite microstrip antenna arrays," in *Proc. Electromagn. Compat.*, 2007, pp. 10–14.

[17] M. A. Setta and C. G. Parini, "Investigating the mutual coupling between mm-wave slot-ring antennas using the FD-TD method," in *Proc. Antenna Technol.: Small Smart Antennas Metamaterials Appl.*, 2007.

[18] A. A. L. Neyestanak, F. Jolani, and M. Dadgarpour, "Mutual coupling reduction between two microstrip patch antennas," in *Proc. Electr. Comput. Eng.*, 2008, pp. 739–742.

[19] I. Ndip., M. Hirte, S. Guttowski, and H. Reichl, "On the integration of a 2.4 GHz ISM band antenna in proximity to transmission lines," in *Proc. Antennas Propag.*, Mar. 23–27, 2009, pp. 2353–2356.

[20] S. Grivet-Talocia, M. Bandinu, F. Canavero, I. Kelander, and P. Kotiranta, "Fast assessment of antenna-PCB coupling in mobile devices: A macromodeling approach," in *Proc. Int. Symp. Electromagn. Compat.*, Jan. 12–16, 2009, pp. 193–196.

[21] Y. Fan and Y. Rahmat-Samii, "Microstrip antennas integrated with electromagnetic band-gap (EBG) structures: a low mutual coupling design for array applications," *IEEE Trans. Antennas Propag.*, vol. 51, no. 10, pp. 2936–2946, Oct. 2003.

[22] F. Ohnimus, I. Ndip, E. Engin, S. Guttowski, and H. Reichl, "Study on shielding effectiveness of mushroom-type electromagnetic bandgap structures in close proximity to patch antennas," in *Proc. Loughborough Antennas Propag. Conf.*, 2009, pp. 737–740.

[23] I. Ndip, H. Reichl, and S. Guttowski, "A novel methodology for defining the boundaries of geometrical discontinuities in electronic packages," in *Proc. Res. Microelectron. Electron.*, 2006, pp. 193–196.

[24] I. Ndip, "Novel methodologies for efficient and accurate modeling and optimization of system-in-package modules for RF/high-speed applications", Ph.D. dissertation, Tech. Univ. Berlin, Berlin, Germany, 2006.

[25] C. A. Balanis, *Antenna Theory – Analysis and Design*, 2nd ed. New York: Wiley, 1997.

[26] R. Suga, H. Nakano, Y. Hirachi, J. Hirokawa, and M. Ando, "Cost-effective 60-GHz antenna package with end-fire radiation for wireless file-transfer system," *IEEE Trans. Microw. Theory Techn.*, vol. 58, no. 12, pp. 3989–3995, Dec. 2010.

Florian Ohnimus was born in Lüneburg, Germany. He received the M.Sc. (Dipl.-Ing.) (Hons.) degree in electrical engineering from the Technical University (TU) of Berlin, Berlin, Germany, in 2007.

Since April 2007, he has been a Research Engineer in the RF and High-Speed System Design Group, Fraunhofer Institute for Reliability and Microintegration and the Research Center for Microperipheric Technologies, Berlin, Germany.

Mr. Ohnimus is the recipient of the "Studienpreis" of Faculty IV of the TU in 2007, the Erwin-Stephan Award from the TU in 2008, and the Best Paper Prize of the Loughborough Antennas and Propagation Conference in 2010.

Gerhard Fotheringham was born in Wiesbaden, Germany. He received the M.Sc. (Dipl.-Mathematiker) degree in mathematics and physics from the Johannes-Gutenberg-Universität, Mainz, Germany, and the Ph.D. (Dr.-Ing.) degree from the Technical University (TU) of Berlin, Berlin, Germany. His Ph.D. thesis was focused on the applications of high-temperature superconductivity in microelectronics.

He was engaged as a Researcher and a Lecturer at TU Berlin, where he is currently a Research Engineer in the RF and High-Speed System Design Group, Fraunhofer Institute for Reliability and Microintegration, Berlin. His research interests include the mathematical modeling and simulation in the fields of microelectronics, microsystems, and microintegration.

Ivan Ndip (M'05) studied electrical engineering at the Technical University (TU) Berlin, Germany. He received the M.Sc. (Dipl.-Ing.) degree, and the Ph.D. (Dr.-Ing.) degree with the highest distinction (*summa cum laude*), in 2002 and 2006, respectively.

In 2002, he joined the Fraunhofer-Institute for Reliability and Microintegration (IZM), Berlin, as a Research Engineer, where he was involved in signal integrity modeling and design of system packages/boards as well as on antenna design and integration. Between 2003 and 2005, he was also affiliated with the Chair for High-Frequency Electronics at the University of Paderborn, Germany. In 2005, he was appointed the Group Manager of RF Modeling and Simulation at Fraunhofer IZM. He developed novel concepts that led to the establishment of a new research group, the RF & High-Speed System Design Group. Since 2006, he has been a Senior Research Engineer and Group Manager of RF & High-Speed System Design at Fraunhofer IZM, where he's responsible for leading a team of research engineers as well as for developing and leading research projects that focus on electromagnetic modeling, design and optimization of RF/high-speed packages/boards/modules, integrated antennas and passive RF front-end components. Since 2008 he has also been a Lecturer in the Department of High-Frequency and Semiconductor System Technologies, School of Electrical Engineering and Computer Sciences, Technical University Berlin. He is currently engaged in teaching courses on Numerical Techniques in Electromagnetics and on Electromagnetic Reliability of Microsystems. He has authored and co-authored more than 100 publications in referred journals and conference proceedings. He has also presented many workshops/tutorials at international conferences in the area of electromagnetic modeling and design for RF/High-speed applications. He is a recipient of six best paper awards at leading international conferences/symposia as well as a recipient of the Tiburtius-Prize, awarded yearly for outstanding Ph.D. dissertations in the state of Berlin, Germany.

Dr. Ndip chairs the signal and power integrity committee of the International Microelectronic and Packaging Society (IMAPS). He is also a member of European Microwave Association (EuMA). He is a reviewer of many international journals and a member of the Technical Program Committee of the IEEE Electrical Design of Advanced Package and Systems Symposium (EDAPS).

A. Ege Engin (M'05) received the B.S. degree in electrical engineering from Middle East Technical University, Ankara, Turkey, in 1998, the M.S. degree in electrical engineering from the University of Paderborn, Paderborn, Germany, in 1998, and the Ph.D. degree (*summa cum laude*) from the University of Hannover, Hannover, Germany, in 2004.

He was a Research Engineer with the Fraunhofer Institute for Reliability and Microintegration, Berlin, Germany. From 2006 to 2008, he was an Assistant Research Director with the Microsystems Packaging Research Center, Georgia Institute of Technology. He is currently an Assistant Professor with the Department of Electrical and Computer Engineering, San Diego State University, San Diego, CA. He has authored or coauthored more than 70 publications in journals and conferences in the areas of signal and power integrity modeling, and simulation. He holds one patent with three pending. He coauthored *Power Integrity Modeling and Design for Semiconductors and Systems* (Englewood Cliffs, NJ: Prentice-Hall, 2007).

Dr. Engin was the recipient of the 2009 Semiconductor Research Corporation Inventor Recognition Award. He coauthored publications that received the Outstanding Poster Paper Award at the 2006 Electronic Components and Technology Conference and the Best Paper of the Session Award of the 2007 International Microelectronics and Packaging Society. He was a Best Paper Award finalist in the Board-Level Design Category, DesignCon 2007.

Stephan Guttowski received the M.Sc. (Dipl.-Ing.) and Ph.D. (Dr.-Ing.) degrees in electrical engineering from the Technical University (TU) of Berlin, Berlin, Germany, in 1994 and 1998, respectively.

From 1998 to 1999, he was a Postdoctoral Research Fellow at Massachusetts Institute of Technology, where he was the Head of the research unit that explored the consequences of the new 42-V-systems on the electromagnetic compatibility within future passenger cars. In 1999, he joined the Research Laboratory for Electric Drives, DaimlerChrysler AG, Berlin, where he was involved with the prediction of electromagnetic emission of electrically driven vehicles. In October 2001, he joined the Fraunhofer Institute for Reliability and Microintegration, Berlin, Germany, where he was the Head of the Advanced System Development Group from 2002 to 2005, and has been the Head of the Department of System Design and Integration, since January 2006. He has authored or coauthored extensively in the area of electrical design of electronic packages and boards for high-performance miniaturized systems.

Herbert Reichl (F'00) received the M.S. and Ph.D. degrees in electrical engineering from the Technical University, Munich, Germany.

He was the founding Director of Fraunhofer Institute for Reliability and Microintegration (IZM), Berlin, Germany, with more than 260 full-time employees—one of the leading institutes in the field of microelectronics and microsystem packaging worldwide. He was also a Professor of Electronic Packaging and Interconnection Technologies, Technical University, Berlin, where he led the Research Center for Microperipheric Technologies. He has authored or coauthored more than 900 papers and six books. For the past two decades, he has been engaged in the development and application of innovative packaging and system integration technologies with activities in the field of material and characterization, design, and simulation as well as high-density interconnect and wafer-level packaging, chip and board interconnection technologies, 3-D-packaging and vertical chip integration, mechatronics, micromechanical systems, reliability and failure analysis, environmental engineering, polymer materials and composites, and polytronic and flexible systems.

Prof. Reichl is a member of the Program Committees and a member of Advisory Boards of a number of national and international conferences. He chairs the SMT/HYBRID/PACKAGING conference and exhibition. He is also the Head of the working group Heterogeneous Integration, Nanoelectronics Platform European Nanoelectronics Initiative Advisory Council and a member of the Scientific Committee of the EUREKA Industrial Initiative MEDEA+. He was awarded with the Order of Merit of the Federal Republic of Germany in 2000. For his eminent contribution to research and development of Fraunhofer-Gesellschaft, he was honored with the highest award of Fraunhofer-Gesellschaft, the "Fraunhofer Muenze" in January 2005. Also in January 2005, the IEEE Components, Packaging and Manufacturing Technology Society awarded him with a Special Presidential Recognition (in recognition of his lifetime of technical achievement in microelectronics as a scholar, mentor, and global leader). In recognition of his contributions to the international electronics industry, he was given the iNEMI International Recognition Award in 2005. In 2006, he was the recipient of the highest German Association for Electrical, Electronic, and Information Technologies award. In 2007, he was honored with the Electronics Manufacturing Technology Award.

Klaus-Dieter Lang (M'09) studied electrical engineering from 1976 to 1981 at Humboldt University (HU) of Berlin, Berlin, Germany, where he received the M.Sc. (Dipl.-Ing.) degree in 1981, and two doctorate degrees (Wire Bonding of Multilayers and Quality Assurance in Assembly Processes), in 1985 and 1989, respectively.

In 1981, he joined the HU as a Researcher and was engaged on microelectronic assembly, packaging, and quality assurance up till 1991. In 1991, he joined the company SLV Hannover to build up a Department for Microelectronic and Optic Components Manufacturing. In 1993, he became Department Manager for Chip Interconnections at Fraunhofer Institute for Reliability and Microintegration (IZM), Berlin. From 1995 to 2000, he has been the Director's Personal Assistant at IZM, where he was responsible for marketing and public relations. From 2001 to 2005, he coordinated the Branch Laboratory "Microsystem Engineering" in Berlin-Adlershof, and from 2003 to 2005, he was the Head of the Department of Photonic and Power System Assembly. Since 2006, he has been the Deputy Director of Fraunhofer IZM. Since February 2011, he has been the Director of Fraunhofer IZM, and also a Professor of Nanointerconnection Technologies at the Technical University Berlin. He is the author and coauthor of three books, and more than 130 publications in the field of wire bonding, microelectronic packaging, microsystems technologies, and chip on board.

Prof. Lang is a member of numerous scientific boards and conference committees. Examples are the SEMI Award Committee, the Scientific Advisory Board of EURIPIDES, the Executive Board of VDE-GMM, and the Scientific Chair of the Conference "Technologies of Printed Circuit Boards" and "SMT/HYBRID/PACKAGING." He is a member of DVS, International Microelectronics and Packaging Society, and plays an active role in the international packaging community as well as in conference organization.